Can oxygen utilization rate be used to track the long-term changes of aerobic respiration in the mesopelagic ocean?

Haichao Guo[1], Iris Kriest[1], Andreas Oschlies[1], and Wolfgang Koeve[1]

[1]GEOMAR Helmholtz Centre for Ocean Research Kiel, 24105, Kiel, Germany

Key Points:

- In the mesopelagic North Atlantic Subtropical Gyre, modelled oxygen utilization rate reproduces changes of the modelled true respiration
- In the mesopelagic Tropical South Atlantic, modelled oxygen utilization rate increases while modelled true respiration decreases
- Changes in the mixing process under global warming may be the main driver of the changing oxygen utilization rate in some parts of the ocean

Corresponding author: Haichao Guo, `hguo@geomar.de`

Abstract

Quantifying possible changes in oceanic aerobic respiration will contribute to the understanding of marine deoxygenation. Here we use a high-resolution Earth system model to investigate the ability of oxygen utilization rate (OUR) to track the temporal change of marine respiration. Results show that in intermediate waters of the North Atlantic Subtropical Gyre (200m-1000m), vertically integrated OUR shows the same trend as the model's vertically integrated true respiration (decrease by around 0.2 $molO_2/m^2/y$) for the time period 1850 to 2100. However, in the mesopelagic Tropical South Atlantic, integrated OUR increases by 0.2 $molO_2/m^2/y$, while the local true respiration decreases by 0.3 $molO_2/m^2/y$. We identify changes in water mass mixing over time, affecting apparent oxygen utilization (AOU) and age in different ways, as one explanation for this divergence. Quantitatively assessing changes in aerobic respiration from OUR in a changing ocean will require accurate knowledge of changes in mixing processes.

Plain Language Summary

The ocean is losing oxygen due to an imbalance in oxygen supply and aerobic respiration. Therefore, monitoring the temporal changes in the aerobic respiration rate is essential to quantitatively understand and project marine oxygen changes. Based on the simulations of an Earth system model, we investigate a diagnostic measure of the respiration rate (oxygen utilization rate, OUR), calculated as the ratio of the gradient of the apparent oxygen utilisation (saturated oxygen concentration minus local oxygen concentration) and seawater age that can be computed from transient abiotic tracers. Results show that in the North Atlantic Subtropical Gyre intermediate water (200m-1000m), vertically integrated OUR shows the same trend (decrease by around 0.2 $molO_2/m^2/y$) with the simulated respiration integral for the time period 1850 to 2100 at the 95% confidence level. However, this finding is not confirmed in the Tropical South Atlantic intermediate water, where the OUR integral increases and the simulated local true respiration integral decreases over time. We propose that the changes in isopycnal mixing, affecting AOU and age in different ways, cause the mismatch between OUR-inferred and true respiration in the latter region in the transient ocean.

1 Introduction

Various Earth system models project rapid and perhaps also accelerating ocean deoxygenation (Bopp et al., 2013; Kwiatkowski et al., 2020). However, the simulated deoxygenation differs considerably from available observations covering the recent 50yrs (Schmidtko et al., 2017; Ito et al., 2017) both in magnitude, and the spatial pattern (Stramma et al., 2012; Oschlies et al., 2018). The explanation for the above differences requires knowledge of respective contributions from changing respiration versus changing ventilation to marine deoxygenation over decades (Oschlies et al., 2018; Robinson, 2019). However, the direct measurements of respiration are still sparse because of methodological limitations (Del Giorgio & Williams, 2005; Robinson, 2019).

Here, we focus on the classic Oxygen Utilization Rate (OUR) method as an indirect measure of marine respiration. OUR is defined as the ratio of the gradient of apparent oxygen utilization (AOU, the difference between saturated oxygen concentration, $[O_2^{sat}]$, and actual oxygen concentration, $[O_2^{obs}]$) and the gradient of seawater age on potential density surfaces (equation 1; Jenkins, 1987). Seawater age is defined as the time elapsed since the water had been last in contact with the atmosphere. In the real ocean, AOU is a readily available property of seawater, while the age of a water mass is typically derived from transient abiotic tracers like sulphur hexafluoride (SF6), chlorofluorocarbons (CFCs, e.g. CFC-11, CFC-12), or radioactive elements (e.g. ^3H, ^{39}Ar, ^{14}C) (Fine, 2011; Fine et al., 2017; Stöven et al., 2015). These age tracers have been inten-

sively measured in the last three decades globally (Fine et al., 2017), which allow, theoretically, the widespread use of OUR.

$$OUR = \mathrm{d}AOU/\mathrm{d}t = \mathrm{d}([O_2^{\mathrm{sat}}] - [O_2^{\mathrm{obs}}])/\mathrm{d}t \qquad (1)$$

Despite several field studies (e.g., Jenkins, 1987; Brea et al., 2004; Sonnerup et al., 2013, 2015, 2019; Álvarez-Salgado et al., 2014) and model studies (e.g., Koeve & Kähler, 2016) on OUR, to our knowledge, no study has attempted to evaluate the potential ability of OUR on tracking the trend of aerobic respiration under the changing climate. In order to address this issue, in the following we employ a high-resolution Earth system model to examine the relationship between OUR and true respiration from 1850 to 2100 under a climate change forcing in two selected study areas in the Atlantic Ocean, where the physical-biogeochemical features differ.

2 Method

2.1 Model description

The model used in this study is the Flexible Ocean and Climate Infrastructure (FOCI) Earth system model (Matthes et al., 2020) coupled to ocean biogeochemistry as detailed by Chien et al. (2022). It includes an atmosphere, a land biosphere, an ocean circulation, a sea-ice, and an ocean biogeochemistry component. The oceanic components apply the ORCA05 grid, corresponding to a tripolar grid with $0.5° \times 0.5°$ nominal horizontal resolution and 46 vertical levels with thicknesses varying from 6 m at the surface to 250 m in the deep ocean. Tracer diffusion is aligned along isopycnals, with a diffusion coefficient of 600 $\mathrm{m^2 s^{-1}}$. The biogeochemical component of FOCI, MOPS (Model of Oceanic Pelagic Stoichiometry) includes nine compartments, namely phytoplankton, zooplankton, particulate detritus (DET), dissolved organic matter (DOM), and phosphate, oxygen, nitrate, dissolved inorganic carbon, and alkalinity (Kriest & Oschlies, 2015; Chien et al., 2022). The effects of iron limitation on marine primary productivity are not included in MOPS. The flux profile of particulate organic matter in MOPS follows a "Martin Curve" (Martin et al., 1987), where the exponent is derived from a constant decay rate (0.05 d^{-1}) and linearly increasing sinking speed (0.0354 $\times z$m/d).

We here describe details on how FOCI simulates ideal age and true respiration rate. The ideal age tracer works like a "clock," which increases one day per day since the water parcel has left the surface. The "clock" is restored to zero when the water reaches the surface of the ocean (Thiele & Sarmiento, 1990). In FOCI, the ideal age is set to zero in the upper 10 m. The remineralization rate in MOPS is temperature-independent and depends only on substrate availability and oxygen concentration. Oxygen concentration constrains remineralization rate only when it is lower than oxygen demand from organic matter degradation, which is not the case for our research sections. Hence, we do not need to account for the oxygen dependence of remineralization in this paper, but refer readers to Chien et al. (2022, Appendix A1) for details. The true respiration rate is the total oxygen consumption for aerobic remineralization of detritus (DET) and dissolved organic matter (DOM, in the model expressed in phosphorus unit) per time unit, as described in Equation 2:

$$R_{\mathrm{true}} = [\lambda'_{\mathrm{DET}} \cdot \max(0, DET - P') + \lambda'_{\mathrm{DOP}} \cdot \max(0, DOP - P')] \cdot R_{\mathrm{O2:P}} \Delta t \qquad (2)$$

where λ'_{DET} (0.05d^{-1}) and λ'_{DOP} (0.17y^{-1}) are the temperature-independent decay rates of DET and DOP, respectively. P' is the concentration threshold, set to $10^{-6} mmol \cdot P \cdot m^{-3}$. P' makes sure that when the concentration of organic matter is lower than $10^{-6} mmol \cdot$

$P \cdot m^{-3}$, the remineralization stops. $R_{O2:P} = 165.08044$ denotes the stoichiometric oxygen demand of aerobic remineralization.

The experimental set-up is detailed by Chien et al. (2022). In brief, the coupled ocean-biogeochemical model was simulated for 500 years under prescribed pre-industrial atmospheric pCO_2 (and other greenhouse gases) and hence climate (piControl-spinup), followed by a 250 years (drift) period with zero carbon dioxide emissions in which atmospheric carbon dioxide concentrations are computed prognostically (esm-piControl-spinup). Afterwards, three transient and pre-industrial control (esm-piControl) simulations were carried out, starting from 230th, 240th, and 250th year of esm-piControl-spinup, respectively (for brevity's sake simply referred to as ensemble members 1, 2, 3, respectively). The transient simulations include 165 years (1850 to 2014) historical (esm-Hist) simulation and 85 years (2015 to 2099) projection under the Shared Socioeconomic Pathways 585 (SSP-585) scenario (esm-ssp-585 Eyring et al., 2016). Here, we only present details of simulation ensemble member 1, but provide the statistical analysis of simulated OUR and true respiration for all ensemble members in the Table 1.

2.2 Model analysis

We confine our analysis to the mesopelagic zone, i.e. depth ranges 200m to 1000m. We consider OUR estimates unreliable in the upper 200m in FOCI. In the upper ocean, besides the zero-age as an upper boundary condition at the surface, also AOU might be substantially modified by other biological activities or physical processes besides respiration (in particular photosynthesis and air-sea gas exchange). In the deep ocean below 1000m, respiration proceeds at very low rate (below 0.4 $mmol/m^3/y$), and only contributes 3% of globally integrated oceanic respiration in the FOCI model.

We select two main research sections, referred to as the North Atlantic Subtropical Gyre (NASG section, 60°W-30°W, 20°N-25°N) and the Tropical South Atlantic (TSA section, 35°W-5°W, 15°S-20°S), respectively (Figure 1). Both sections approximately fit the criteria for selecting sections used by Jenkins (1987): sections follow the flow (Figure S1) and are approximately perpendicular to isolines of ideal age and AOU. In addition, the NASG region is one of the regions projected to suffer the most significant reduction of net primary production in the climate projections, though with the large uncertainties (Kwiatkowski et al., 2020; Tagliabue et al., 2021). This might impact local respiration rates and oxygen concentrations.

Along the chosen sections, we compare the diagnosed OUR integral and the true respiration rate integral in the mesopelagic zone rather than on certain density surfaces. We notice the sharp change of density surface depth in the transient simulations (e.g., in the NASG section, the depth of potential density surface 26.5 kg/m^3 increases from 257.1 ± 51.4 to 420.7 ± 4.3 m from 1850 to 2099), which might induce significant changes in the true respiration rate on the respective density surfaces (Figure S2). These changes on moving isopycnals may mislead the analysis of how the biology-induced respiration evolves under changing climate. Hence we explore trends of vertically integrated changes for the depth range 200 to 1000m

We derive the integrals of true respiration rate and OUR from 200m to 1000m as follows. Firstly, we calculate the potential density from potential temperature, salinity, and reference pressure (set to 0 decibar) using the 1980 UNESCO International Equation of State (Millero & Poisson, 1981), and remap data from z-coordinates to sigma0-coordinates. The OUR is calculated for every 0.1 kg/m^3 density surface interval from 24.1 to 28.0 kg/m^3 by using the linear least square regression of AOU versus ideal age. We also calculate the area-weighted mean true respiration rate and mean depth for each density surface. Afterwards, we remap OUR and mean true respiration rate onto z-coordinates using the area-weighted z-depth of the corresponding density surfaces. Finally, the vertical integral is obtained as the sum of the grid-box thickness times the variable (OUR
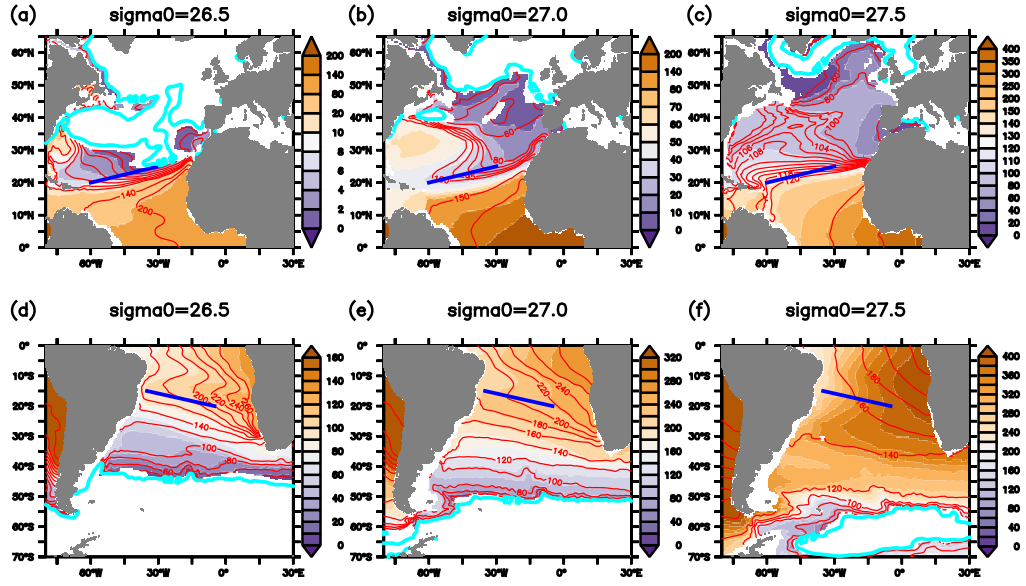
Figure 1. Distributions of ideal age (shading), AOU (red lines), and outcrop locations (light-blue lines) in the North and the South Atlantic Ocean on three isopycnal surfaces. We use the last decade's mean in the esm-piControl simulation and exclude the waters above hemispheric winter mixing depth. Winter surface density outcrops are calculated from March (northern hemisphere) and September (southern hemisphere) mean temperature and salinity. Blue lines represent chosen research sections.

or mean true respiration rate) at each grid point, which is detailed in the supplementary material Text S1. The transformation of coordinates forth and back, fortunately, does not induce biases on either the vertical distribution of true respiration rate or the trend of integrated true respiration rate (Figure S3). For convenience, in the following part, we refer to the integral of OUR and true respiration rate from 200m to 1000m as "OUR" and "true respiration", respectively.

3 Results and discussion

OUR underestimates true respiration in the NASG section by around 1.9 fold (Figure 2a), and most of the underestimation occurs in the upper ocean (Figure 2b). This underestimate might be caused by the spatial heterogeneity of the respiration rate on isopycnals, as found for idealized isopycnals with prescribed patterns of respiration (Koeve & Kähler, 2016). High respiration rates occur near the outcrops (shallower ocean) due to the high availability of substrates and low sinking speed of detritus. However, mixing with nearby surface waters allows the imprint of respiration, AOU, to quickly escape to the atmosphere. On the other hand, respiration far from outcrops (deeper ocean) can be well-preserved as AOU because of smaller mixing losses to surface waters. However, the respiration rate in deeper waters is often much lower because much organic matter has already been consumed in the water column above, and because the sinking speed of particulate organic matter increases with depth (Berelson, 2001). In contrast to respiration, the water aging rate is the same everywhere. Therefore, more idealized age tracer is preserved at isopycnals compared to AOU, and consequently the OUR diagnosed from the gradient ratio is smaller than true respiration rate. The underestimate of OUR compared to the true respiration, and the vertical distribution of their difference has also been found in the other two ensemble members with similar magnitude (Table 1, Figure S4ab, S5ab).

At the 95% confidence level, the esm-piControl results show that OUR slightly decreases by 0.241 ± 0.239 $mmol/m^2/y^2$, while the true respiration increases by 0.282 ± 0.191 $mmol/m^2/y^2$ along the NASG section. However, this diverging trend of OUR and true respiration in the esm-piControl is not repeated in the other ensemble members (Table 1, Figure S4, S5), which indicates that the divergence in the esm-piControl simulation from ensemble member 1 may not be induced by the drift but perhaps by the multi-decadal or even longer variability (with small magnitude) in the FOCI model (Matthes et al., 2020). The Pearson correlation coefficient between the diagnosed OUR and the true respiration in esm-piControl is 0.48.

The true respiration in the NASG section shows a long term decreasing trend along with global warming in the transient simulations (Figure 2d). Here we use the transient simulation minus esm-piControl to remove the trend in the latter and isolate the climate change signal. The true respiration decreases by 0.872 ± 0.268 $mmol/m^2/y^2$ from 1850 to 2100, indicating a decline of up to 10.6 % of local mesopelagic respiration. The trend is the same in the other two ensemble members at the 95% confidence level.

For the strong climate change scenario simulated here, OUR is suitable to track the long-term trend of local true respiration along the NASG section (Figure 2). OUR decreases by 0.802 ± 0.333 $mmol/m^2/y^2$, which is overlapped with true respiration changes. Besides, the Pearson correlation coefficient between the diagnosed OUR and the true respiration is 0.54 for the transient scenario. In the other two ensemble members, the trends of true respiration and OUR versus time also overlap at the 95% confidence level (Table 1).

Now we describe the OUR performance in our second study region, the TSA section (Figure 3). The vertically integrated OUR here amounts to 83.3% of the true respiration in the esm-piControl simulation (Figure 3a), and the underestimation occurs
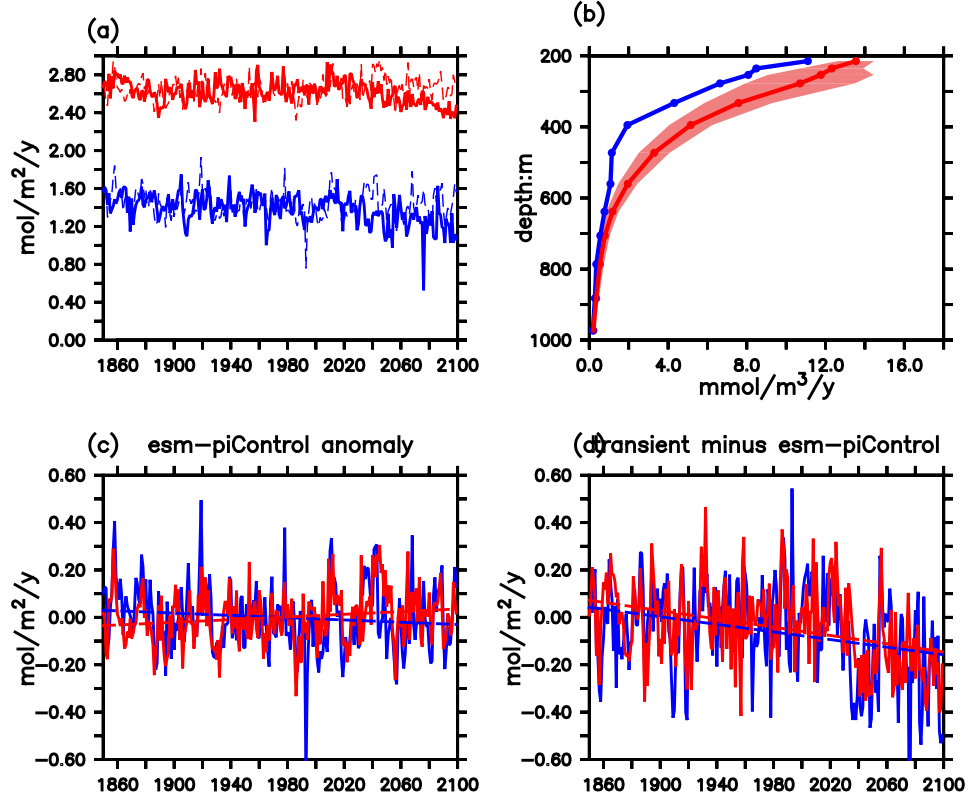
Figure 2. Comparison between vertically integrated OUR and the true respiration rates (200 - 1000m) along the NASG section (see blue line in Figure 1a) in simulation ensemble member 1. Panel (a) shows absolute integrated OUR (blue) and true respiration (red) from the transient simulation (solid) and the esm-piControl simulation (dashed). Panel (b) is the vertical distribution of OUR (blue) and true respiration rate (red) in the last year of the esm-piControl simulation. The shading indicates one standard deviation. All r^2 values of the linear regressions of AOU against ideal age on density surfaces are above 0.92. Panel (c) shows the integrated OUR (thick blue line) and true respiration (thick red line) anomalies relative to the respective time-averaged values of the esm-piControl simulation. The thin solid lines are the linear least square regression lines of integrated OUR anomalies (blue) and integrated true respiration anomalies (red) over time. (d) shows the transient minus esm-piControl integrated OUR (blue) and true respiration (red), and their linear least square regression lines over time.
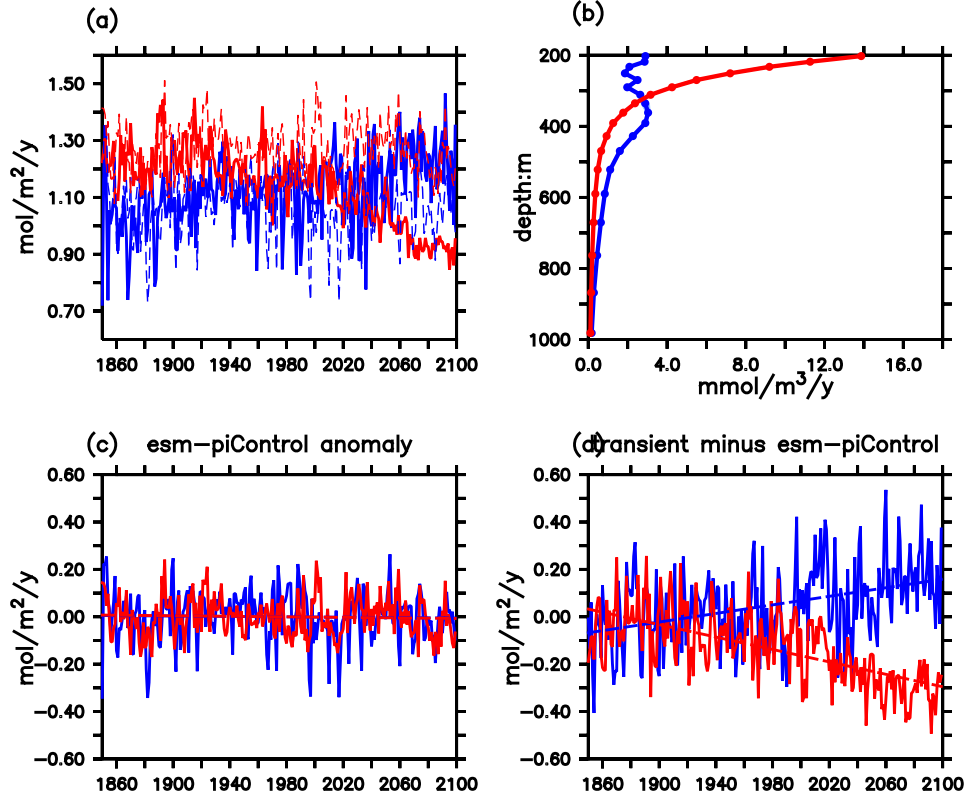
Figure 3. As Figure 2, but for the TSA section (see blue line in Figure 1d). In panel (b), all r^2 values of the linear regressions of AOU against ideal age on density surfaces are above 0.94.

between 200m and 300m (Figure 3b). The reason for the underestimate might be similar to what we proposed for the NASG section above. Below around 320m, however, OUR overestimates true respiration rate and it even increases between 300m to 400m (Figure 3b). Both OUR and true respiration do not change over time in the esm-piControl simulation (Figure 3c), but the Pearson correlation coefficient between them is only 0.193. In the transient minus esm-piControl, OUR and true respiration show a significant diverging trend (Figure 3d). True respiration decreases by $1.311 \pm 0.197 \ mmol/m^2/y^2$, but OUR increases significantly by $0.905 \pm 0.257 \ mmol/m^2/y^2$. The other two ensemble members show similar features (Table 1, Figure S6,S7). To sum up the above results, we propose that along the TSA section the trend of OUR is not mainly determined by changes of local respiration.

One explanation for the discrepancy of temporal trends of OUR and true respiration may be found in the different effects of mixing on AOU and age distributions along isopycnals, which may steepen or flatten the slope of OUR. For better clarification, we rewrite

$$OUR = R_{\mathrm{true}} + OUR_{\mathrm{mixing}} \tag{3}$$

Table 1. Ratio of OUR and true respiration rate, slope of true respiration and OUR over time and their 95% confidence interval, and Pearson correlation coefficient between OUR and true respiration (with p-value below 0.05).

Region	simulations	true respiration/OUR	trend of true respiration ($mmol/m^2/y^2$)[a]	trend of OUR ($mmol/m^2/y^2$)[a]	correlation coefficient between true respiration and OUR
NASG	esm-piControl				
	ensemble member 1	1.9	0.282±0.191	-0.241 ±0.239	0.48
	ensemble member 2	1.9	-0.139±0.207	-0.289±0.246	0.51
	ensemble member 3	1.9	0.433±0.205	-0.040±0.258	0.45
	transient minus esm-piControl				
	ensemble member 1	1.9	-0.872±0.268	-0.802±0.333	0.54
	ensemble member 2	1.9	-0.833±0.296	-0.844±0.357	0.54
	ensemble member 3	1.9	-0.981±0.272	-0.754±0.362	0.55
TSA	esm-piControl				
	ensemble member 1	1.2	/	/	0.19
	ensemble member 2	1.2	0.206±0.137	/	0.13
	ensemble member 3	1.2	0.191±0.150	-0.316±0.188	/
	transient minus esm-piControl[b]				
	ensemble member 1	1.0	-1.311±0.197	0.905±0.257	-0.19
	ensemble member 2	1.0	-1.783±0.200	0.520±0.268	/
	ensemble member 3	1.0	-1.323±0.182	0.826±0.257	-0.17

[a] For trends: positive number means increase and negative number means decrease.

224 in which, R_{true} is local aerobic respiration, and OUR_{mixing} is OUR induced by all
225 processes other than local aerobic respiration. We propose that the value of OUR_{mixing}
226 is determined mainly by mixing of waters from different origin and age, yielding imprints
227 of ocean biogeochemistry outside the section under investigation. While local respira-
228 tion (R_{true}) might change due to anthropogenic affects, also OUR_{mixing} can be affected
229 by global warming via changes in ocean circulation and remote biogeochemical processes.
230 Depending on sections under investigation, the local respiration might be either the main
231 (e.g., in the NASG section in our study) or a minor driver (e.g., in the TSA section in
232 our study) of long-term OUR change.

233 To reliably infer changes of respiration from OUR under global warming, it is re-
234 quired to remove the mixing-induced contributions to AOU and age. However, to our
235 knowledge quantitatively assessing the mixing-induced AOU and age in a transient ocean
236 is still a challenge. This has been addressed in several studies by applying the Optimal
237 Multi-Parameter (OMP) analysis (e.g., Brea et al., 2004; Álvarez-Salgado et al., 2014).
238 However, this method requires that the properties (e.g., potential temperature, salinity)
239 of water masses in their formation regions are constant. In a changing ocean, the OMP
240 method cannot straightforwardly be used to infer the contributions of R_{true} and OUR_{mixing}
241 to transient OUR.

4 Conclusions

243 Our study confirms the potential ability of OUR to track the trends of true res-
244 piration during the time period of 1850 and 2100, and may hence contribute to our un-
245 derstanding of drivers of ocean deoxygenation in parts of the ocean. However, there is
246 also a risk that temporal trends diagnosed from OUR can be an unreliable indicator of
247 trends in true respiration, and may even be of opposite sign to trends of true respira-
248 tion in other parts of the ocean (as in the example of the TSA). In a changing climate,
249 this discrepancy can arise from temporal variations in ocean mixing and circulation that
250 can map remote effects on ocean biogeochemistry and age tracers onto the local OUR.
251 The mixing-induced OUR possibly counteracts or even reverses the respiration-induced
252 OUR changes in sections under investigation. Quantitatively assessing changes in aer-
253 obic respiration from OUR in a changing ocean requires the separation of mixing-induced
254 AOU and age.

5 Data availability statement

256 The model code is provided by Chien et al. (2022) at https://doi.org/10.5281/zenodo.6772175.
257 The full model outputs used in this paper (only for variables potential temperature, salin-
258 ity, dissolved oxygen concentration, ideal age, and true respiration rate) are too large (above
259 130 GB for each ensemble member) to be provided in an online repository, therefore we
260 provide only the last 10 years of esm-piControl simulations for reproducing partial re-

sults. These model outputs together with the scripts for data processing are available
at: https://hdl.handle.net/20.500.12085/e7d53204-df0c-4973-8628-63dad7dd140.

References

Álvarez-Salgado, X. A., Álvarez, M., Brea, S., Mémery, L., & Messias, M. (2014). Mineralization of biogenic materials in the water masses of the south atlantic ocean. ii: Stoichiometric ratios and mineralization rates. *Progress in Oceanography*, *123*, 24–37.

Berelson, W. M. (2001). Particle settling rates increase with depth in the ocean. *Deep Sea Research Part II: Topical Studies in Oceanography*, *49*(1-3), 237–251.

Bopp, L., Resplandy, L., Orr, J. C., Doney, S. C., Dunne, J. P., Gehlen, M., . . . others (2013). Multiple stressors of ocean ecosystems in the 21st century: projections with cmip5 models. *Biogeosciences*, *10*(10), 6225–6245.

Brea, S., Álvarez-Salgado, X. A., Álvarez, M., Pérez, F. F., Mémery, L., Mercier, H., & Messias, M.-J. (2004). Nutrient mineralization rates and ratios in the eastern south atlantic. *Journal of Geophysical Research: Oceans*, *109*(C5).

Chien, C.-T., Durgadoo, J. V., Ehlert, D., Frenger, I., Keller, D. P., Koeve, W., . . . others (2022). Foci-mops v1–integration of marine biogeochemistry within the flexible ocean and climate infrastructure version 1 (foci 1) earth system model. *Geoscientific Model Development Discussions*, 1–58.

Del Giorgio, P., & Williams, P. (2005). *Respiration in aquatic ecosystems*. OUP Oxford.

Eyring, V., Bony, S., Meehl, G. A., Senior, C. A., Stevens, B., Stouffer, R. J., & Taylor, K. E. (2016). Overview of the coupled model intercomparison project phase 6 (cmip6) experimental design and organization. *Geoscientific Model Development*, *9*(5), 1937–1958.

Fine, R. A. (2011). Observations of cfcs and sf6 as ocean tracers. *Annual review of marine science*, *3*, 173–195.

Fine, R. A., Peacock, S., Maltrud, M. E., & Bryan, F. O. (2017). A new look at ocean ventilation time scales and their uncertainties. *Journal of Geophysical Research: Oceans*, *122*(5), 3771–3798.

Ito, T., Minobe, S., Long, M. C., & Deutsch, C. (2017). Upper ocean o2 trends: 1958–2015. *Geophysical Research Letters*, *44*(9), 4214–4223.

Jenkins, W. J. (1987). 3 h and 3 he in the beta triangle: Observations of gyre ventilation and oxygen utilization rates. *Journal of Physical Oceanography*, *17*(6), 763–783.

Koeve, W., & Kähler, P. (2016). Oxygen utilization rate (our) underestimates ocean respiration: A model study. *Global Biogeochemical Cycles*, *30*(8), 1166–1182.

Kriest, I., & Oschlies, A. (2015). Mops-1.0: towards a model for the regulation of the global oceanic nitrogen budget by marine biogeochemical processes. *Geoscientific Model Development*, *8*(9), 2929–2957.

Kwiatkowski, L., Torres, O., Bopp, L., Aumont, O., Chamberlain, M., Christian, J. R., . . . others (2020). Twenty-first century ocean warming, acidification, deoxygenation, and upper-ocean nutrient and primary production decline from cmip6 model projections. *Biogeosciences*, *17*(13), 3439–3470.

Martin, J. H., Knauer, G. A., Karl, D. M., & Broenkow, W. W. (1987). Vertex: carbon cycling in the northeast pacific. *Deep Sea Research Part A. Oceanographic Research Papers*, *34*(2), 267–285.

Matthes, K., Biastoch, A., Wahl, S., Harlaß, J., Martin, T., Brücher, T., . . . others (2020). The flexible ocean and climate infrastructure version 1 (foci1): mean state and variability. *Geoscientific Model Development*, *13*(6), 2533–2568.

Millero, F. J., & Poisson, A. (1981). International one-atmosphere equation of state of seawater. *Deep Sea Research Part A. Oceanographic Research Papers*, *28*(6), 625–629.

Oschlies, A., Brandt, P., Stramma, L., & Schmidtko, S. (2018). Drivers and mechanisms of ocean deoxygenation. *Nature Geoscience*, *11*(7), 467–473.

Robinson, C. (2019). Microbial respiration, the engine of ocean deoxygenation. *Frontiers in Marine Science*, 533.

Schmidtko, S., Stramma, L., & Visbeck, M. (2017). Decline in global oceanic oxygen content during the past five decades. *Nature*, *542*(7641), 335–339.

Sonnerup, R. E., Chang, B. X., Warner, M. J., & Mordy, C. W. (2019). Timescales of ventilation and consumption of oxygen and fixed nitrogen in the eastern tropical south pacific oxygen deficient zone from transient tracers. *Deep Sea Research Part I: Oceanographic Research Papers*, *151*, 103080.

Sonnerup, R. E., Mecking, S., & Bullister, J. L. (2013). Transit time distributions and oxygen utilization rates in the northeast pacific ocean from chlorofluorocarbons and sulfur hexafluoride. *Deep Sea Research Part I: Oceanographic Research Papers*, *72*, 61–71.

Sonnerup, R. E., Mecking, S., Bullister, J. L., & Warner, M. J. (2015). Transit time distributions and oxygen utilization rates from chlorofluorocarbons and sulfur hexafluoride in the s outheast p acific o cean. *Journal of Geophysical Research: Oceans*, *120*(5), 3761–3776.

Stöven, T., Tanhua, T., Hoppema, M., & Bullister, J. (2015). Perspectives of transient tracer applications and limiting cases. *Ocean Science*, *11*(5), 699–718.

Stramma, L., Oschlies, A., & Schmidtko, S. (2012). Mismatch between observed and modeled trends in dissolved upper-ocean oxygen over the last 50 yr. *Biogeosciences*, *9*(10), 4045–4057.

Tagliabue, A., Kwiatkowski, L., Bopp, L., Butenschön, M., Cheung, W., Lengaigne, M., & Vialard, J. (2021). Persistent uncertainties in ocean net primary production climate change projections at regional scales raise challenges for assessing impacts on ecosystem services. *Frontiers in Climate*, 149.

Thiele, G., & Sarmiento, J. (1990). Tracer dating and ocean ventilation. *Journal of Geophysical Research: Oceans*, *95*(C6), 9377–9391.